Cutting Performance of Bionic Cutting tools Based on Surface Microstructures of Blood Clams in Dry Cutting of CFRP

Changtang You
Xiamen University
Chaoping Xie
Xiamen University
Xuyang Chu
Xiamen University
Wei Zhou
Xiamen University
Guolong Zhao
Nanjing University of Aeronautics and Astronautics
Yunsong Lian (lianys@xmu.edu.cn)

Original Article

Keywords: CFRP, bionic cutting tools, microstructures, blood clams, turning

DOI: https://doi.org/10.21203/rs.3.rs-36540/v1

Abstract

Carbon fibre reinforced polymer (CFRP) composites are widely used in high-tech industries like the automobile and aerospace sectors, but the wear resistance of tools is one of the most significant restrictions in machining CFRP. In this study, bionic cutting tools based on surface microstructures of blood clams were fabricated to improve the dry cutting performance of CFRP. Three types of bionic cutting tools with different size parameters were applied in dry cutting test. The three-axis cutting forces and the cutting temperature of the processed workpiece were measured. The average friction coefficient between the rake face and the chip was calculated, and the morphology of the tools wear were observed. The results showed that bionic microstructures with appropriate size parameters can extremely improve the cutting performance of CFRP for tool in turning.

1 Introduction

Carbon fibre reinforced polymer (CFRP) composites have excellent specific mechanical properties, low density, high damping ability, good dimensional stability and good corrosion resistance, etc. [1,2]. These materials are therefore widely used in high-tech industries like the automobile and aerospace sectors. Even they take up over 50% of the structural weight of some aircraft. However, the CFRPs machining is often difficult. One of the reason why they are a difficult-to-cut material is that the high abrasive wear effect of the carbon fibres on the cutting tool [3]. And the CFRPs are normally cannot be allowed to use any cutting fluid in CFRPs machining due to the hygroscopicity, which aggravates the tool wear and high cutting temperature furthermore.

Many researchers have already characterized that the cutting edge rounding and the flank wear are the two main kinds of tool wear appeared in secondary cutting edge of one-shot drill bit in drilling CFRP [4,5]. And the hole surface quality strictly worse because of the damages induced by tool wear. In order to predict and reduce the values of the flank wear, Kim et al. [6] constructed the tool wear progression model considering the fiber orientation and the radial depth of cut in end milling of CFRP. The estimation results showed that CFRP milling conditions must have larger radial depth of cut. Liang et al. [7] proposed a novel method of improving tool life by pre running-in and the effectiveness was verified by drilling tests. That is to say, the conventional cutting tools is usually not the best choice to machining good quality features in CFRPs unless using some certain methods. A effective approach to improve machining quality is that making the single cutting thickness in the reasonable range [8,9]. On the other hand, applying internal coolant holes at specific position and using minimum quantity lubrication (MQL), the tool wear is also effectively reduced and hole surface quality is greatly improved [10]. Cutting tool producers and researchers have developed numerous cutting tools with special geometries for CFRP manufacturers. Li et al. [11] presented a detailed experimental investigation of unidirectional fibre reinforced polymer (UD-CFRP) orthogonal cutting and chip removal mechanisms in the case of using a specially designed solid tungsten carbide tool. It can be stated that advanced geometry cutting tools are necessary in order to effectively and appropriately machine required quality features when working with CFRP composites.

Recently, the non-smooth surface effect has great potential to improve the lubrication, reduce the friction and enhance wear resistance of friction pairs [12, 13, 14]. Thus, surface texturing proved to be one of the promising techniques which helped in the improvement of wear resistance of cutting tools. Sugihara et al. [15] developed cutting tools with dimple-shaped textures having different dimensions and arrays, generated on the tool rake face. The experimental results show that microdimples on the rake face of a cutting tool effectively suppress the crater wear in cutting medium carbon steels, and the effect can be obtained even under dry cutting conditions. Niketh et al. [16] manufactured a novel drill tool having microtextures at the flute and margin side and it is used to reduce the sliding friction while machining Ti6Al4V. It is found that surfaces with micro grooves showed a lower wear depth of 400 μm while compared to non-textured surfaces which recorded a maximum wear depth of 1150 μm. Liu et al. [17] investigated the wear resistance of flank-face textured tools by dry cutting tests on the green alumina ceramics with these flank-face textured tools and a conventional WC/Co carbide tool. The flank wear of the flank-face textured tools was significantly reduced compared with that of the conventional one, and the flank-face textured tools with micro-scale grooves on the flank face parallel to the main cutting edge had the most improved flank wear resistance. Xing et al. [18] irradiated Al_2O_3/TiC cutting tools rake face by a femtosecond laser. Then dry cutting tests were carried out with these pretreated tools and conventional tools on hardened steel. They found that the laser pretreated tools increased the adhesions of chips on the rake face, but they can significantly improve the wear resistance of the rake face. On the other hand, Chen et al. [19] indicated that the surface quality of CFRP machined by the micro-textured milling tools was also improved over that by the conventional one.

Over billions of years of evolution, a large number of organisms generally have excellent functions of adhesion reduction, drag reduction and wear resistance [20, 21]. Wang et al. [22] investigated the influences of smooth and bio-inspired surfaces on tribological properties of the carbon-fiber-reinforced polyetheretherketone (CFRPEEK) coupled with stainless steel 316L under natural seawater lubrication. The results show that the specimen with ellipsoidal pits (surface characteristic of the cytister bengalensis) has the best anti-wear performance, followed by the specimen with triangular pits (surface characteristic of the snake). Zhang et al. [23] optimized the shape of dimple surface texture under unidirectional sliding, and a numerical approach developed based on a Genetic Algorithm to improve the tribological performance. It was illustrated that textures of the bullet and fish shapes had lower friction coefficient than those of circular shape.

As a typical natural biological mineralization material, molluscan shells have excellent wear-resistance properties. Tian et al. [24] investigated the influence of surface morphology (rib distribution on the shell), structure (rib coupled with nodules) and material (organic matter) on the anti-wear performance of the molluscan *Scapharca subcrenata* shell. All three were found to exert significant effects on the shell's wear-resistance ability. Zhang et al. [25] generated two kinds of bionic units, the bionic strip unit (inspirited by the shell structure) and the bionic pit unit (inspirited by the dung beetle) on the surface of the specimens. The two kinds of units can improve the resistance to sliding wear dramatically.

Hence, in this work, in order to convenient observation, the bionic cutting tools based on the surface microstructure of blood clams were fabricated to machining CFRP in the turning for reducing the tool-chip friction, improving the wear resistance and prolonging the service life of tools.

2 Experiments

2.1 Selection of bionic objects

Blood clams mainly grows in the shallow sea and sand along the coast or near the land. Thus, the the surface will be impacted by surrounding sediments which driven by water flows. But there is no obvious wear on the surface due to the surface morphology of the blood clams, a geometric network structure with interlaced longitudinal grooves and transverse grooves, which makes it resistant to erosion and abrasion. The microstructure of blood clams was observed by an ordinary optical microscope and the dimensions were measured by a confocal microscope as shown in Figure 1 and Figure 2(b) respectively. In this study, the blood clams were selected as a bionic prototype and applied to tools to study the cutting performance with this bionic structure.

Figure 1 The macrostructures of blood clams: (a) ten times magnification, (b) thirty times magnification

Figure 2 The local microstructures of blood clams: (a) microstructures observed by an ordinary optical microscope, (b) microstructures observed by a confocal microscope

2.2 Preparation of bionic cutting tools

The tools tested in this research were 13 × 13 × 4.5 mm YS8 (WC / TiC / Co) carbide tools. The physical properties of YS8 cemented carbide are shown in Table 1. We used an abrasive polisher to polish the rake face of tools so that its surface roughness Ra was less than 10 nm, and then cleaned it in an ultrasonic cleaner with alcohol and acetone for 20 minutes respectively.

Table 1 Physical properties of the YS8 ultra-fine grained cemented carbide blade

Cutting tool	Hardness (HRA)	Flexural strength (MPa)	Density (g/cm^3)
YS8	92.5	1720	13.9
Young's Modulus (GPa)		Thermal expansion coefficient(10^{-6} ºC)	Poisson's ratio
550	5.5		0.27

In this study, three groups of bionic tools were prepared by laser micromachining technology. The model of the laser marking machine used in the test is RFL-100W, as shown in Figure 3(a). And the morphological diagrams of three kinds of bionic tool obtained by laser processing are shown in the Figure 3 (b), (c), (d). Three groups of bionic tools and one groups of conventional non-textured tools NT were subjected to cutting tests.

2.3 Cutting tests

The dry cutting test was performed on a CA6136 engine lathe. Its front angle γ_0, back angle α_0, main declination angle K_r and blade inclination angle λ_s were -5°, 5°, 45°, 0° respectively. The workpiece material used in the experiment was an CFRP round bar with a diameter of 55 mm.

The experimental image of the cutting test is shown in Figure 4. The cutting force was measured by a dynamic force measurement system (Kistler 9272) fixed on the engine lathe, and then the force data was changed from an amplifier to a computer data acquisition system. Three-axis forces recorded by the dynamic force measurement system are main cutting force, radial force, and feed force respectively. A thermal imager (C640) was used to observe the cutting temperature of the tool-chip interface during cutting.

Figure 3 RFL-100W Laser marking machine and three-dimensional morphology of the rake face of three kinds of bionic tools after machining: (a) RFL-100W Laser marking machine, (b) bionic tool T8, (c) bionic tool T20, (d) bionic tool T25

Figure 4 Turning test site layout: (a) lathe processing device, (b) data processing

3 Results And Discussions

3.1 Cutting forces

As shown in the Figure 5 is a table of the three-axis cutting force of the four tools under the cutting conditions of v=160 m/min, f=0.2 mm/r and a_p=0.4 mm. It can be seen from the figure that the three-axis cutting force of the bionic tools T8, T20 and T25 is lower than that of the ordinary non-textured tool NT, especially T20, and the three-axis cutting force is smaller than that of the conventional non-textured tool NT. The main cutting force, radial force and feed force were reduced by 16.45%, 31.90% and 25.31% respectively. In addition, generally speaking, the cutting force of the four tools for cutting CFRP is relatively small, but the cutting force oscillates greatly during the cutting process. This is because CFRP is a difficult-to-cut material, and its bar material structure is laminated fibres. The process of turning CFRP is accompanied by the breakage of fibres and the cutting of new fibre layers, so the cutting force is in a continuous oscillation cycle. This continuous oscillation has a considerable impact on the tool, that is, to improve the tool performance is critical for cutting CFRP materials.

Figure 5 Three-axis cutting forces of four tools (v=160 m/min, f=0.2 mm/r, a_p=0.4 mm): (a) main cutting force, (b) radial force, (c) feed force

Figure 6 shows the change curve of the three-axis cutting force of the four tools at a cutting speed of 80-180 m/min (f=0.2 mm/r, a_p=0.4 mm) to cut CFRP. Judging from the changing trend of cutting force, it generally shows a trend of decreasing first and then increasing, the reason being. In general, the cutting force of the four tools in cutting CFRP in the tested cutting speed range is relatively small, and it can be clearly seen that the three-axis cutting forces of the bionic tools T8 and T20 are the smallest. When the cutting speed is 80-120 m/min, the main cutting force of T8 and T20 is reduced by 5.70%~11.78% and 4.29%~11.42% respectively compared to the conventional non-textured tool NT, and the radial force is reduced by 5.66%~13.08% and 2.94%~18.74%, the feed force is reduced by 2.06%~24.13% and -1.87%~16.36%; when the cutting speed is large, in the range of 140-180 m/min, T8 and T20 main The cutting force is reduced by 9.46%~17.79% and 10.56%~16.45%, the radial force is reduced by 21.38%~28.51% and 28.88%~33.92%, and the feed force is reduced by 15.58%~23.22% and 13.51%~26.48%. It can be seen that the three-axis cutting force of the bionic tools T8 and T20 drops significantly when the cutting speed is large, indicating that these two bionic tools have a more prominent role in reducing the cutting force at higher cutting speeds.

Figure 6 Under the conditions of different cutting speeds, the change of the three-axis cutting force experienced by the four tools: (a) main cutting force, (b) radial force, (c) feed force

In addition, the T25 bionic tool also has the effect of reducing the cutting force of the tool in the higher cutting speed range of 140-180 m/min. Compared with the conventional non-textured tool, the NT main cutting force is reduced by 8.77%, 7.34% and 10.23%, radial force decreased by 15.07%, 14.83% and 19.09% respectively, and feed force decreased by 9.17%, 13.85% and 12.80% respectively. It can be seen that the bionic microstructure is suitable for cutting at a higher cutting speed, and can improve the cutting performance of the tool during high-speed cutting.

3.2 Cutting temperature

During the cutting process, FLUKE TI32 portable infrared camera was used to measure the cutting temperature of the tool. Figure 7 is the infrared thermal image of four tools cutting CFRP when the cutting speed is 140 m/min. It can be seen from the figure that under this cutting condition, the maximum temperature of the tool tip of the conventional non-textured tool is 119.1ºC, while the maximum temperature of the tip of the bionic tool T8 is 77.0ºC, which is 35.35% lower than that of the conventional non-textured tool.

Figure 7 Infrared thermography of conventional non-textured tool NT and bionic tool T8 in dry cutting of CFRP (v=140 m/min, f=0.2 mm/r, a_p=0.4 mm): (a) conventional non-textured tool NT, (b) bionic tool T8

Figure 8 shows the cutting temperature changes of four different tools in the cutting speed range of 80-180 m/min. On the whole, the cutting temperature of the four tools shows a trend of decreasing first and then increasing with the increase of cutting speed. The minimum temperature appears at 120 m/min and 140 m/min. It can be clearly seen from the figure that at any cutting speed, the cooling effect of the bionic tools T8 and T20 is obvious, and the bionic tool T25 has a better cooling effect when the cutting speed is higher. T8 and T20 in the test cutting speed range, compared with conventional non-textured cutting tools, the cutting temperature was reduced by 10.25%~20.42% and 11.82%~32.67% respectively. The temperature reduction effect of T25 at a higher cutting speed of 140-180 m/min also reached 6.31%~13.43%. It can be seen that the effects of the three bionic tools at lower cutting speeds are more significant. It can be seen that the presence of microstructures on bionic cutting tools based on surface microstructures of blood clams can effectively improve the heat dissipation efficiency of the friction interface, so that the temperature rise of the tool tip during cutting can be significantly lower than that of the non-textured texture. Therefore, when cutting a hard-to-cut material such as CFRP with a micro-structured tool with surface microstructures of blood clams, the tool surface will have a lower temperature than the conventional tool, and the purpose of extending the tool life is achieved.

Figure 8 Cutting temperature of four kinds of tool at different cutting speeds (f=0.2 mm/r, a_p=0.4 mm)

3.3 Average friction coefficient

According to the theory of metal cutting, in the process of metal cutting, the relationship among the cutting tool geometry angles, the radial force F_Y and the main cutting force F_Z satisfies Formula (1), and then the calculation formula of the average friction coefficient μ of the tool-chip contact surface on the tool rake face can be derived.

$$\mu = \tan(\beta) = \tan(\gamma_0 + \arctan F_Y / F_Z) \quad (1)$$

Where μ-average friction coefficient, β-friction angel, γ_0- tool rake angel, F_Y-radial force and F_Z-main cutting force.

The data obtained by the cutting test and the Formula (1) give the average friction coefficient of the tool-chip contact surface of the four tools at different cutting speeds, and the curve of its change with cutting speed is shown in Figure 9. On the whole, the average friction coefficient on the rake face of the tool shows a downward trend with the increase of cutting speed. It can be seen from the figure that the bionic tool T8 has a certain friction reduction effect at the cutting speed v=180 m/min, and the average friction coefficient at other cutting speeds is not much different from that of conventional non-textured tools. The bionic tool T20 has a good friction reduction effect when the cutting speed $v \geq 120$ m/min, especially when the cutting speed v=140 m/min, the friction coefficient is reduced by 21.02% compared to NT, and the friction reduction effect is significant. In contrast, the bionic tool T25 not only does not have a good anti-friction effect, but even increases the friction between the rake face and the chip, making the average friction coefficient increase. It can be seen that the proper microstructures of the surface of the bionic tool

can play the anti-friction effect under certain cutting conditions and play a positive role in improving the cutting performance of the tool.

Figure 9 Average friction coefficient of four kinds of tools turning CFRP at different cutting speeds (f=0.2 mm/r, a_p=0.4 mm)

3.4 Chip adhesion and wear

The main reasons for tool wear are excessive contact pressure between the tool and the workpiece and excessive temperature on the contact surface. In high-speed cutting, a large amount of cutting heat is generated between the workpiece and the tool. The temperature of the contact area between the workpiece and the tool is high and the pressure is high. In this state, the fresh chip surface formed by cutting often has a strong chemical activity and atomic adsorption force, it is easy to cause adhesion on the contact surface between the tool and the workpiece. The adhesion material will take off part of the tool material, causing damage to the tool and causing bond wear. This is the main form of wear in cutting CFRP materials.

Figure 10 shows the two-dimensional bonding morphology of the rake face of conventional non-textured tool NT and bionic tool T8 and T20 dry cutting CFRP and the distribution diagram of H element in epoxy resin under the cutting conditions of v=180 m/min, f=0.2 mm/r, a_p= 0.4 mm. It can be seen from the figure that these two kinds of cutters have a more obvious black bond near the cutting edge of the rake face area, which is in sharp contrast with the tool material. The cutter mainly focuses on bond wear. Observing Figure 10 (a)-(f), it can be seen that the size and scope of the non-textured tool NT block bond are significantly larger than the bionic tools T8 and T20, indicating the bond wear of the conventional non-textured tool NT more seriously, the bionic tool can effectively reduce the size of the worn area on the rake face of the tool. Because T8 and T20 have a lower degree of bond wear, the average friction coefficient of T8 and T20 rake faces is somewhat lower than that of NT, thereby increasing the tool life.

Figure 10 Two-dimensional bonding morphology and the H element distribution on the rake faces of three kinds of tools (v=180 m/min, f=0.2 mm/r, a_p=0.4 mm): (a) NT two-dimensional bonding morphology, (b) H element distribution of NT, (c) T20 two-dimensional bonding morphology, (d) H element distribution of T20, (e) T8 two-dimensional bonding morphology, (f) H element distribution of T8

4 Conclusions

In this work, the conventional non-textured tool NT, the bionic tools T8, T20, T25 were applied to turning carbon fiber reinforced polymer (CFRP) under six turning speeds. The conclusions are as follows:

(1) The bionic microstructure is suitable for cutting at a higher cutting speed, and can improve the cutting performance of the tool during high-speed cutting. In the range of 140-180 m/min, the main cutting force of T8, T20 and T25 is reduced up to 17.79%, 16.45% and 10.23%. The radial force is reduced up to

28.51%, 33.92% and 19.09% respectively. The feed force is reduced up to 23.22%, 26.48% and 12.80% respectively.

(2) The presence of microstructures on bionic cutting tools based on surface microstructures of blood clams can effectively improve the heat dissipation efficiency of the friction interface. The cutting temperature of bionic cutting tools T8 and T20 was reduced by 10.25%~20.42% and 11.82%~32.67% respectively compared with conventional non-textured cutting tools in the test cutting speed range. The temperature reduction effect of T25 at a higher cutting speed of 140-180 m/min also reached 6.31%~13.43%.

(3) The proper microstructures of the surface of the bionic tool can play the anti-friction effect under certain cutting conditions. The bionic tool T20 has a good friction reduction effect when the cutting speed, especially when the cutting speed v=140 m/min. The friction coefficient is reduced by 21.02% compared to NT. But the bionic tool T25 increases the friction between the rake face and the chip.

(4) The bionic tool can effectively reduce the size of the worn area on the rake face of the tool seriously compared with the conventional non-textured tool NT.

5 Declaration

Acknowledgements

The authors sincerely thanks to the support from Department of Mechanical and Electrical Engineering, Xiamen University, and Jiangsu Key Laboratory of Precision and Micro-Manufacturing Technology.

Funding

This work was supported by the National Natural Science Foundation of China (Grant No. 51505399 and 51975496), the Natural Science Foundation of Fujian Province of China (Grant No. 2017J05088), and Jiangsu Key Laboratory of Precision and Micro-Manufacturing Technology.

Availability of data and materials

The datasets supporting the conclusions of this article are included within the article.

Authors' contributions

The author' contributions are as follows: Yun-Song Lian was in charge of the whole trial; Chang-Tang You wrote the manuscript; Chao-Ping Xie assisted with sampling and laboratory analyses; Xu-Yang Chu, Wei Zhou and Guo-Long Zhao guided the experiments. All authors read and approved the final manuscript.

Competing interests

The authors declare no competing financial interests.

Consent for publication

Not applicable.

Ethics approval and consent to participate

Not applicable.

References

1. Y Takeshi, O Takayuki, S Hiroyuki. Temperature measurement of cutting tool and machined surface layer in milling of CFRP. *International Journal of Machine Tools and Manufacture*, 2013, 70: 63-69.
2. B S Aymen, M Ali, E M Mohamed. Rigorous treatment of dry cutting of FRP-interface consumption concept: a review. *International Journal of Mechanical Sciences*, 2014, 83: 1-29.
3. N Geier, J P Davim, T Szalay. Advanced cutting tools and technologies for drilling carbon fibre reinforced polymer (CFRP) composites: a review. *Composites Part A-Applied Science and Manufacturing*, 2019, 125: 105552.
4. Z Y Jia, G J Bi, F J Wang, et al. The research of machining mechanism of carbon fiber reinforced plastic. *Journal of Mechanical Engineering*, 2018, 54(23): 199-208. (in Chinese)
5. F J Wang, J W Yin, Z Y Jia, et al. Measurement and analysis of cutting force, temperature and cutting-induced top-layer damage in edge trimming of CFRPs. *Journal of Mechanical Engineering*, 2018, 54(03): 186-195. (in Chinese)
6. F J Wang, B W Qian, D Cheng, et al. Wear of one-shot drill bit in drilling CFRP and novel method for tool wear reduction. *Journal of Mechanical Engineering*, 2018, 54(15): 171-179. (in Chinese)
7. F J Wang, B W Qian, Z Y Jia, et al. Secondary cutting edge wear of one-shot drill bit in drilling CFRP and its impact on hole quality. *Composite Structures*, 2017, 178: 341-352.
8. S Gaugel, P Sripathy, A Haeger, et al. A comparative study on tool wear and laminate damage in drilling of carbon-fiber reinforced polymers (CFRP). *Composite Structures*, 2016, 155: 173-183.
9. M Kim, M Lee, G Cho, et al. Effect of the fiber orientation and the radial depth of cut on the flank wear in end milling of CFRP. *International Journal of Precision Engineering and Manufacturing*, 2020. (in press)
10. X Liang, D Wu. Tribological properties of carbon-fibre-reinforced plastic against tungsten carbide under dry condition. *Tribology International*, 2019, 134: 118-128.
11. H Li, X D Qin, G Y He, et al. Price M. Investigation of chip formation and fracture toughness in orthogonal cutting of UD-CFRP. *International Journal of Advanced Manufacturing Technology*, 2016, 82(5-8): 1079-88.
12. J Kümmel, D Braun, J Gibmeier, et al. Study on micro texturing of uncoated cemented carbide cutting tools for wear improvement and built-up edge stabilisation. *Journal of Materials Processing Technology*, 2015, 215: 62-70.

13. D Vasumathy, A Meena, M Duraiselvam. Experimental study on evaluating the effect of micro textured tools in turning AISI 316 austenitic stainless steel. *Procedia Engineering*, 2017, 184: 50-7.
14. C C Zhou, X H Guo, K D Zhang, et al. The coupling effect of micro-groove textures and nanofluids on cutting performance of uncoated cemented carbide tools in milling Ti-6Al-4V. *Journal of Materials Processing Technology*, 2019, 271: 36-45.
15. T Sugihara, T Enomoto. Performance of cutting tools with dimple textured surfaces: a comparative study of different texture patterns. *Procedia Engineering*, 2017, 49: 52-60.
16. S Niketh, G L Samuel. Drilling performance of micro textured tools under dry, wet and MQL condition. *Journal of Manufacturing Processes*, 2018, 32: 254-268.
17. Y Y Liu, J X Deng, F F Wu, et al. Wear resistance of carbide tools with textured flank-face in dry cutting of green alumina ceramics. *Wear*, 2017, 372: 91-103.
18. Y Q Xing, J X Deng, K D Zhang, et al. Effect of femtosecond laser pretreatment on wear resistance of Al2O3/TiC ceramic tools in dry cutting. *International Journal of Refractory Metals and Hard Materials*, 2014, 43: 291-301.
19. Y D Chen, X H Guo, K D Zhang, et al. Study on the surface quality of CFRP machined by micro-textured milling tools. *Journal of Manufacturing Processes*, 2019, 37: 114-123.
20. H A Abdel-Aal, M E Mansori, H Zahouani. A comparative study of frictional response of shed snakeskin and human skin. *Wear*, 2017, 376–377: 281-294.
21. G J Liu, Z C Yuan, Z Z Qiu, et al. A brief review of bio-inspired surface technology and application toward underwater drag reduction. *Ocean Engineering*, 2020, 199: 106962.
22. Z Q Wang, Q Fu, R J K Wood, et al. Influence of bionic non-smooth surface texture on tribological characteristics of carbon-fiber-reinforced polyetheretherketone under seawater lubrication. *Tribology International*, 2020, 144: 106100.
23. H Zhang, M Hua, G Z Dong, et al. Optimization of texture shape based on genetic algorithm under unidirectional sliding. *Tribology International*, 2017, 115: 222-232.
24. L M Tian, X M Tian, Y C Wang, et al. Anti-wear properties of the molluscan shell Scapharca subcrenata: Influence of surface morphology, structure and organic material on the elementary wear process. *Materials Science and Engineering C-Materials for Biological Applications*, 2014, 41: 7-14.
25. H F Zhang, T Zhou, H Zhou, et al. Effects of different bionic units coupling on the sliding wear of gray cast iron. *Surface and Coatings Technology*, 2017, 309: 96-105.

Tables

Table 1

Physical properties of the YS8 ultra-fine grained cemented carbide blade.

Cutting tool	Hardness (HRA)	Flexural strength (MPa)	Density (g/cm^3)	Young's Modulus (GPa)	Thermal expansion coefficient(10^{-6}°C)	Poisson's ratio
YS8	92.5	1720	13.9	550	5.5	0.27

Figures

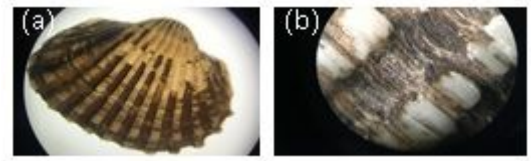

Figure 1

The macrostructures of blood clams: (a) ten times magnification, (b) thirty times magnification

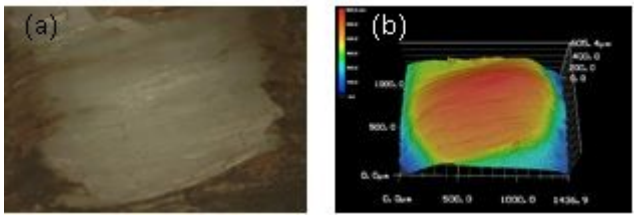

Figure 2

The local microstructures of blood clams: (a) microstructures observed by an ordinary optical microscope, (b) microstructures observed by a confocal microscope

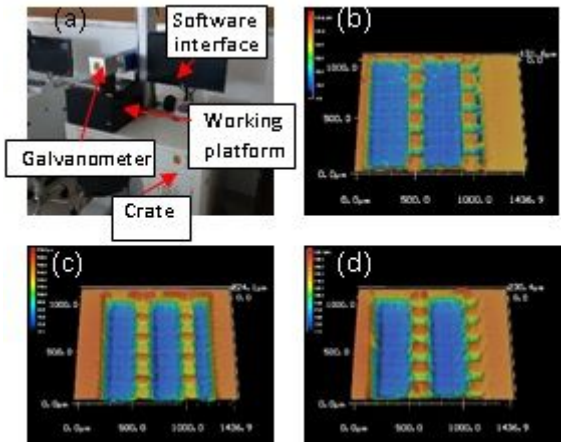

Figure 3

RFL-100W Laser marking machine and three-dimensional morphology of the rake face of three kinds of bionic tools after machining: (a) RFL-100W Laser marking machine, (b) bionic tool T8, (c) bionic tool T20, (d) bionic tool T25

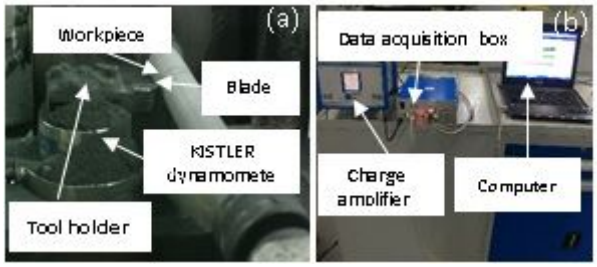

Figure 4

Turning test site layout: (a) lathe processing device, (b) data processing

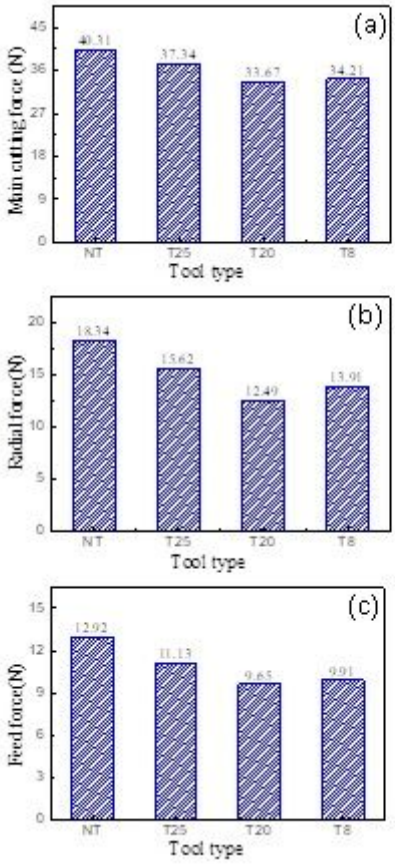

Figure 5

Three-axis cutting forces of four tools (v=160 m/min, f=0.2 mm/r, ap=0.4 mm): (a) main cutting force, (b) radial force, (c) feed force

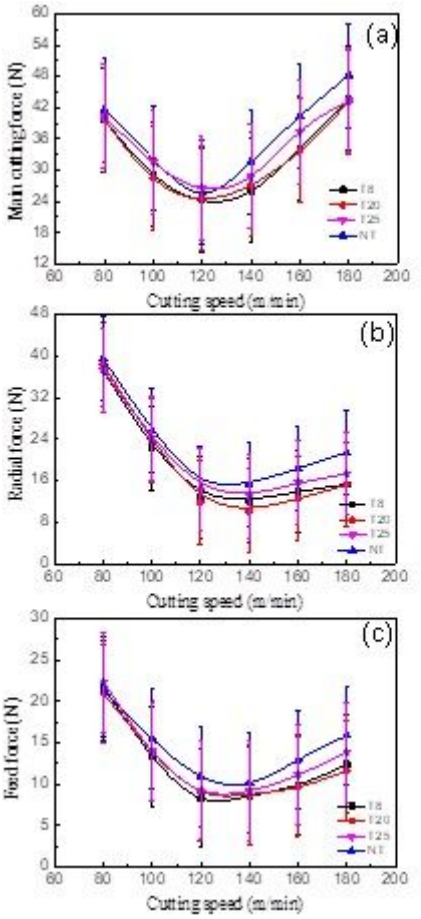

Figure 6

Under the conditions of different cutting speeds, the change of the three-axis cutting force experienced by the four tools: (a) main cutting force, (b) radial force, (c) feed force

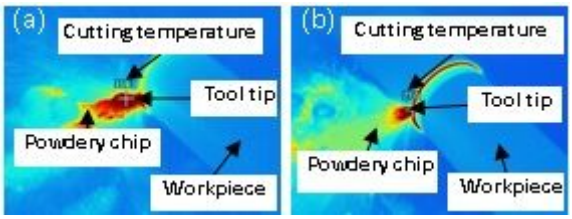

Figure 7

Infrared thermography of conventional non-textured tool NT and bionic tool T8 in dry cutting of CFRP (v=140 m/min, f=0.2 mm/r, ap=0.4 mm): (a) conventional non-textured tool NT, (b) bionic tool T8

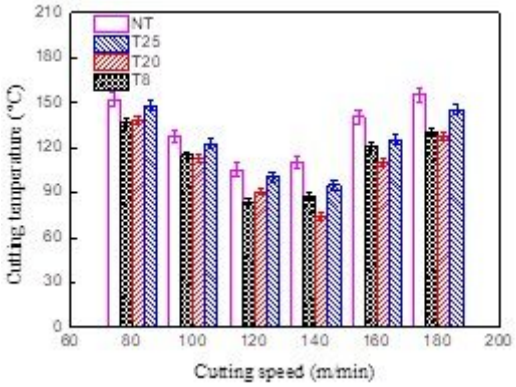

Figure 8

Cutting temperature of four kinds of tool at different cutting speeds (f=0.2 mm/r, ap=0.4 mm)

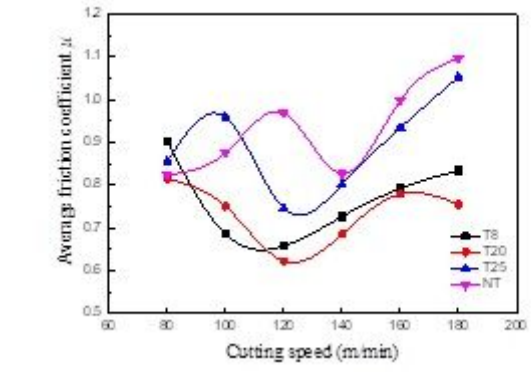

Figure 9

Average friction coefficient of four kinds of tools turning CFRP at different cutting speeds (f=0.2 mm/r, ap=0.4 mm)

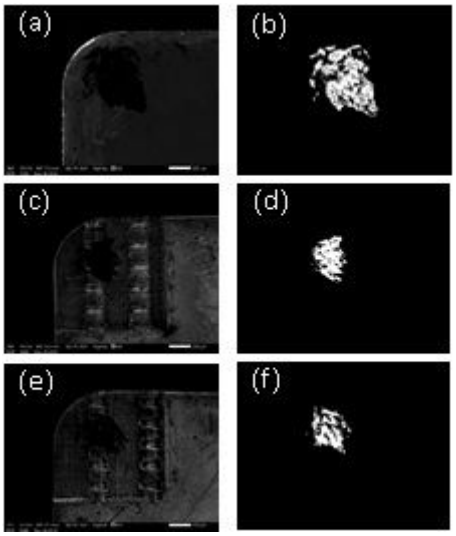

Figure 10

Two-dimensional bonding morphology and the H element distribution on the rake faces of three kinds of tools (v=180 m/min, f=0.2 mm/r, ap=0.4 mm): (a) NT two-dimensional bonding morphology, (b) H element distribution of NT, (c) T20 two-dimensional bonding morphology, (d) H element distribution of T20, (e) T8 two-dimensional bonding morphology, (f) H element distribution of T8